

# Investigation of Light Transmission Efficiency in ITER Hard X-Ray Monitor

Shin KAJITA, Santosh P. PANDYA<sup>1)</sup>, Richard O'CONNOR<sup>2)</sup>,  
Robin BARNSLEY<sup>2)</sup> and Huxford ROGER<sup>3)</sup>

*Institute of Materials and Systems for Sustainability, Nagoya University, Nagoya 464-8603, Japan*

<sup>1)</sup>*Institute for Plasma Research, Near Indira Bridge, Bhat, Gandhinagar - 382428, India*

<sup>2)</sup>*ITER Organization, Route de Vinon-sur-Verdon, CS 90 046, 13067 St. Paul Lez Durance Cedex, France*

<sup>3)</sup>*RBH Optics, Burgess Hill, England, United Kingdom*

(Received 16 September 2021 / Accepted 31 October 2021)

A Hard X-ray monitor (HXRM) diagnostic system is being designed for ITER tokamak and will be utilized to detect runaway electrons for the safe operation of the tokamak. Runaway electrons produce X-ray photons by means of thick target and/or thin target bremsstrahlung emission process. In this diagnostic measurement system, the X-ray photons interact with scintillator detector volume and generate secondary UV-photons by luminescence. These UV-photons from the scintillator-crystal guided through the optics and detected by photomultiplier tubes. The light collection efficiency from the scintillator-crystals and light transmission efficiency of the optics determines the detectable energy range of X-rays and energy resolution. In this letter, we perform ray-tracing simulations of the luminescence to optical fiber bundle to assess light collection efficiency from the scintillator-crystal and show the effect on the total light coupling efficiency of the system.

© 2021 The Japan Society of Plasma Science and Nuclear Fusion Research

Keywords: ITER, hard X-ray monitor, scintillator, ray tracing, runaway electron

DOI: 10.1585/pfr.16.1302106

Production of runaway electrons (RE) in tokamak is an important issue particularly for the safe operation of large size tokamak that confines mega amperes of plasma current. Gamma-ray / Hard X-ray monitor (HXRM) is well-known methods that detect bremsstrahlung emission from the REs to infer RE energy, runaway beam current, and its profile during disruption [1, 2]. An HXRM system will be installed in ITER, which will measure typically MeV range bremsstrahlung emission from REs [3–5]. The HXRM system will be used to support the commissioning of the disruption mitigation system and also to build operation scenarios for RE avoidance. Recently, a numerical tool has been developed to simulate the expected signal in ITER HXRM system and optimize the design parameters [3]. One of the concerns for the development of the HXRM for ITER is the light coupling efficiency of the scintillator and the transmission of optics. The lowest energy detection threshold depends on the efficiency of the scintillator and transmission of optics [3, 5]. However, there has been no valid calculation to assess the efficiency of scintillator, even though the factor is crucial. In this letter, for the ITER HXRM, we model the light coupling efficiency of scintillator to an optical fiber bundle using a ray tracing analysis by including the absorption and reflection in the scintillator crystal. By using the ray tracing analysis, it is possible to investigate reflection of rays on

the surfaces, absorption in the crystal, and the geometrical effects such as taper-shaped scintillator. Also, we show the transmission of optics and total throughput of the system, and discuss the expected theoretical performance of HXRM based on these values.

A schematic in Fig. 1 shows the major components in the HXRM system of ITER. Two scintillator crystals are placed behind the diagnostic first wall (DFW). Photons produced in the scintillator crystal are transferred using an optical fiber bundle. At the vacuum closure plate, the optical fiber is coupled to another optical fiber via double windows and lens assembly, and photons are detected with photomultiplier tubes (PMTs). It should be noted that the operational/functional role of the HXRM is limited to only a *non-nuclear phase* of ITER plasma operation; the optical

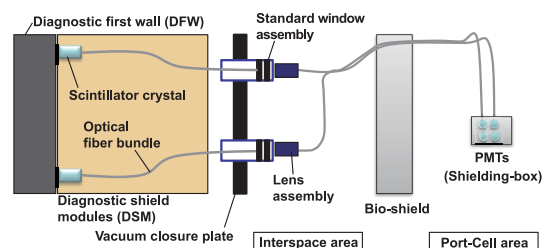


Fig. 1 A schematic of the major components of ITER HXRM system.

author's e-mail: kajita.shin@nagoya-u.jp

fiber can be used in the non-nuclear phase using hydrogen/helium gas discharges.

Total transmission of the optics is determined by losses in the optics: losses on the two optical fiber surfaces, fiber attenuation, losses on the window assembly and lens assembly, and PMT coupling efficiency (Fig. 1). Anti-reflection coating surface is assumed for surface loss. Then, the overall transmission is estimated to be 17.8% from the in-vessel optical fiber bundle to the PMT.

Figure 2 (a) shows a schematic of the model used in ray tracing simulation, which is done using the commercial ray tracing software LightTools, which has been used for modeling of stray light or performance of illumination in ITER [6, 7]. The candidate material for the scintillator

crystal is La-GPS:Ce, which has a high refractive index of 1.825, and assumed that the cylindrical crystal volume corresponds to a uniform light source in the ray tracing model. The scintillator crystal is surrounded by a covered material for better light reflection properties; in actual situation, it will be covered with a aluminum foil/coating/lap. In the ray tracing model, the optical property can be changed from absorber to optical reflector (diffuse or specular). Concerning the reflection on the crystal surface, the reflection feature strongly depends on whether there is a gap between the scintillator crystal and the cover material. If there is a gap (gap model), the reflection on the scintillator surface dominates as will be discussed later. To simulate the case without gap (no-gap model), we built a model where the reflectance can be controlled totally. For this, in LightTools, the scintillator (source) material is immersed to another material that can control the surface reflection property using *immersion manager*. This is because the reflection of a source cannot be changed in LightTools. We can apply different reflection properties, which corresponds to the reflection property of the covered material, to the immersing cylinder. In both models, the reflection of the covered material is assumed to be diffuse.

A receiver is located at one side of the source, and an angular filter is equipped on the receiver to be able to receive photons only within the angle defined by the numerical aperture (NA) of optical fiber bundle, which is assumed to be 0.28 in this study. Another side surface is covered with the covered material. Figure 2 (b) shows a typical intensity profile at the receiver. The efficiency of the receiver is assessed by averaging the intensity profile without considering the intensity distribution.

There are three influential factors to the efficiency: transmission of scintillator, opening angle of fiber, and refractive index of scintillator. Transmission has been discussed by measuring the intensity for different scintillators with different lengths [8]. In Ref. [8], from the fitting of the light yield as a function of the sample height, it was obtained that light loss coefficient was  $0.53 \text{ cm}^{-1}$ . In LightTools, we used transparency defined as

$$T = \exp(-\lambda L), \tag{1}$$

where  $\lambda$  is the mean free path of photons and  $L$  is the travel length. When using  $\lambda = 0.53 \text{ cm}^{-1}$ ,  $T = 0.588$  at  $L = 1 \text{ cm}$ .

However, the light loss coefficient in Ref. [8] is not necessarily corresponds to the absorption coefficient, because this value was obtained just from the fitting procedure with a simple function. The rays do not travel in a straight line but follow a convoluted path, so that the actual length could be more or less than  $2h$ , where  $h$  is the crystal height. Thus, the transmission value should be carefully taken into consideration.

In addition to the transmission of scintillator, opening angle of fiber is also an influential factor. The opening angle is determined by the NA of fiber. When NA is 0.28, the half opening angle decreases from 90 degree to 16.24 de-

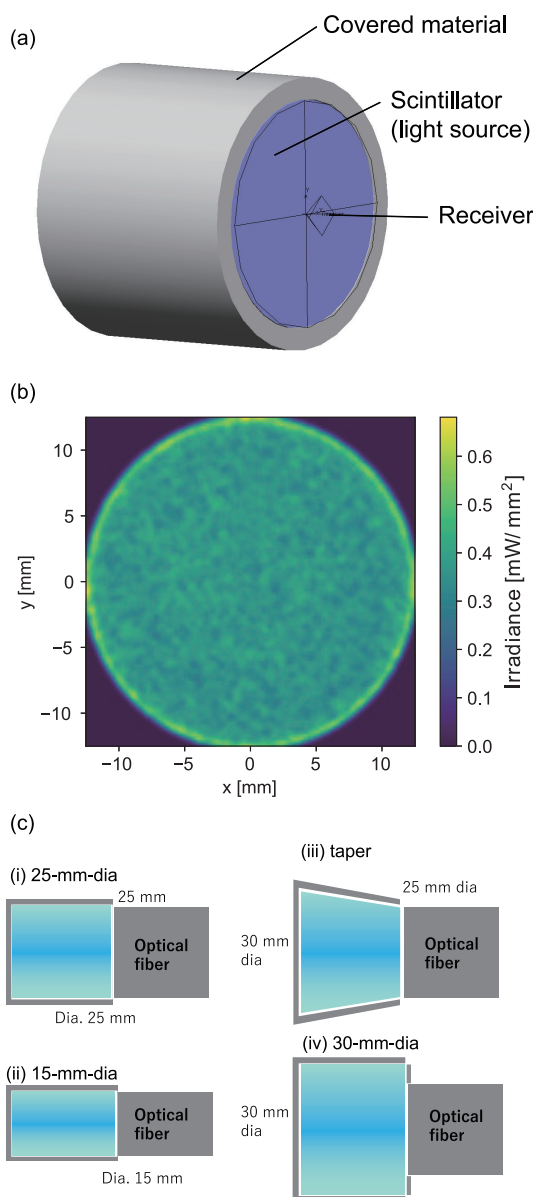


Fig. 2 (a) A schematic of the simulation model, (b) a typical image at the receiver (fiber surface), and (c) schematics of four scintillator models.

gree. As a consequence, the solid angle is decreased from  $2\pi$  to 0.25 (3.9%). Furthermore, because the refractive index of the scintillator is high, the effective opening angle decreases. The effective opening angle decreases from 16.24 to 8.90 degree at the refractive index of 1.825. (The solid angle decreases by 70% from 251 msr to 75.3 msr).

Four different models shown in Fig. 2 (c) are compared. First model is the standard one which has 25 mm in length and 25 mm in diameter. Size of the fiber is also 25 mm in diameter. Second one is a small scintillator that has 25 mm in length and 15 mm in diameter. Third one is a taper shaped scintillator: one side has 30 mm in diameter and the other size connected to the fiber is 25 mm in diameter. Final one is a scintillator that has 25 mm in length and 30 mm in diameter. The fiber bundle size is 25 mm in diameter.

Figure 3 (a) summarizes the transmission  $T$  dependences of the scintillator efficiency (fraction of photons reached the receiver (optical fiber) from the source) with the gap and no-gap models at different reflection,  $R$  ( $R = 98\%$  and  $0\%$ ). Here,  $R = 98\%$  corresponds the case where the scintillator is covered by a reflective material, while  $R = 0\%$  corresponds the case without a cover or an absorber material. In all the models, the efficiency increases with increasing  $T$ . With the gap model at  $R = 98\%$ , the

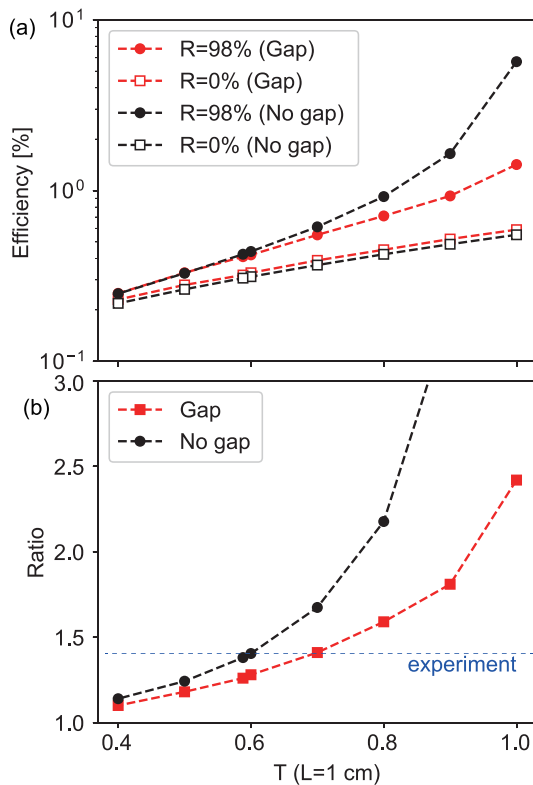


Fig. 3 (a) Transmittance dependences of the collection efficiency with  $R = 0$  and  $98\%$  and (b) the ratio of the collection efficiencies at  $R = 98\%$  to that at  $R = 0\%$ . Here,  $T$  is the transmission at  $L = 1$  cm.

efficiency increased from 0.25 to 1.42% from  $T = 0.4$  to unity. The efficiency of the no-gap model at  $R = 98\%$  is higher than the other models. Figure 3 (b) shows the ratio of the efficiency at  $R = 98\%$  to that at  $R = 0\%$ . The ratio also increased with  $T$  and the ratio of the gap model is higher than no-gap model. Pandya S.P. experimentally investigated the variation in the photon output from the scintillator when covering the scintillator with white silicon tape or black absorber [5]. He has revealed that the intensity increased by 40% when the scintillator was covered with the silicon tape. In Fig. 3, the ratio becomes 1.4 when  $T = 0.7$  with the gap model and  $T = 0.6$  with no-gap model, suggesting that  $T$  was slightly greater than or almost comparable to the reported value in [8].

It seems that the two configurations are quite different especially when  $T$  is high. At  $T = 1.0$ , the efficiency was 5.68% at  $R = 98\%$  when using no-gap model, while it became 1.65% when gap model was used. With gap model, a lot of rays suffered from internal reflection and were “caught” inside the cylinder and were not be able to escape, as shown in Fig. 4 (a). Figure 4 (b) shows an en-

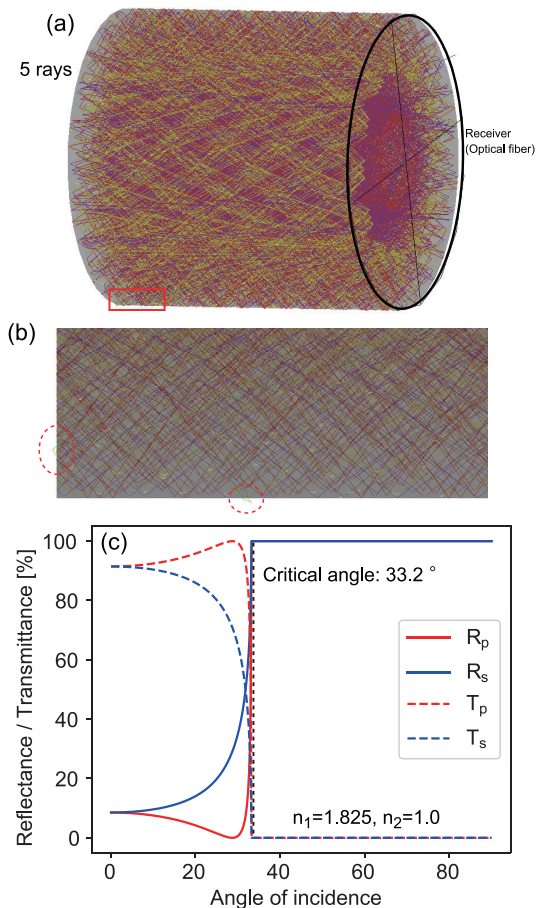


Fig. 4 (a) Five rays in the gap model with  $T = 1.0$  (no absorption), (b) an image expanding in the region marked with a red square in (a), and (c) reflectance / transmittance as a function of the angle of incidence for s and p polarizations when  $n_1 = 1.825$  and  $n_2 = 1.0$ .

larged image of the red square region in Fig. 4 (a). At the cylinder surface, specular reflection occurred almost all the time. Clear diffuse reflectance at the reflector surface can only be identified two cases marked with dotted red circles in Fig. 4 (b). When checking ray report, it was found that more than half of rays were terminated after reaching the maximum number of hits (the number of surface interaction) of 1000. Figure 4 (c) shows reflectance and transmittance for s and p polarization from the scintillator to the air, of which the refractive index is  $n_1 = 1.825$  and  $n_2 = 1.0$ , respectively. When the incident angle is less than the critical angle, which is defined as  $\sin^{-1}(n_2/n_1)$  and is  $33.2^\circ$ , the reflectance is determined by Fresnel formulae [9]. On the other hand, if the incident angle is greater than the critical angle, the rays will be totally trapped inside the cylinder. Without the gap, on the other hand, the reflection property was determined by the cover. If the cover has a diffuse reflectance, the rays can change the angle and break the trapping. It is difficult to say which model we should adopt. If the material has a thin film deposition, it is likely that no-gap model is more realistic. However, if the material is covered by polytetrafluoroethylene (PTFE) tape or aluminium foil, it is likely that the gap between the covered material and the surface is not much shorter than the wavelength; gap model is more plausible.

Then, it would be instructive to know how much is the impact of difference between the gap and no-gap models. When the material is transparent, the difference could be significant, say more than double from Fig. 3 (b). However, at  $T = 0.7$ , the difference was much less (0.55%:0.61%), and the impact will be minor. We will use the gap model hereafter.

In Fig. 5, the efficiency of the four models with different  $T$  values is shown. The efficiency is 0.55% at  $T = 0.7$ , and it decreases to 0.41% at  $T = 0.588$ . For the small diameter model, the relative power becomes 36% of the standard model, because the total area that collect photons was smaller. Concerning the taper model, the efficiency is

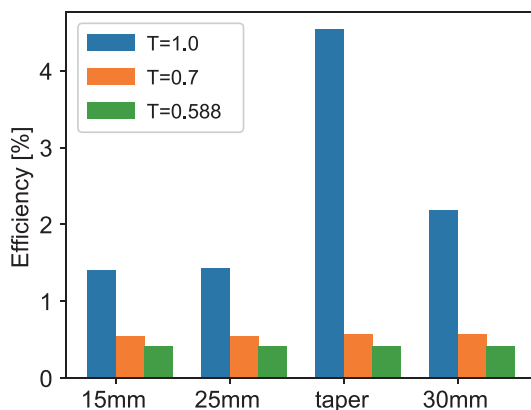


Fig. 5 Collection efficiency for the four different models at three different  $T$  (transmission for  $L = 1$  cm).

much higher than the standard model at  $T = 1$ ; however, the difference will be diminished with decreasing  $T$ . The difference was only 4% at  $T = 0.7$  and 1% at  $T = 0.588$ . For 30-mm-long large scintillator model, the efficiency is 50% higher than the standard model at  $T = 1$ ; however, the difference is also diminished with increasing  $T$  similar to the taper cases. The difference is only 5% at  $T = 0.7$  and 2% at  $T = 0.588$ .

The optical transmission efficiency has a direct impact on the performance of the ITER HXRM on the following two parameters: (i) the low energy detection threshold of the HXR-photons and (ii) energy resolution of the system. The overall optical efficiency of the ITER HXRM system can be calculated by the transmission of optics (17.8%) times the efficiency of scintillator (0.41 - 0.55%) and is in the range of 0.073 - 0.098%. The lower optical transmission efficiency provides higher HXR-photon energy detection threshold and a poor energy resolution. Since the role of the ITER HXRM system is to measure the RE energy, essentially the poor energy resolution should not be a problem as the bremsstrahlung emission is a continuum and measurement interest is not to resolve and individual HXR/Gamma-photon lines. On the other hand, the theoretical HXR-energy detection threshold of the HXRM diagnostic system corresponding to the overall optical transmission efficiency of 0.073 - 0.098% is estimated close to 1 MeV and to be validated experimentally as a future scope of the work. With this detection threshold, energy resolution, detector response function and a prior knowledge of the bremsstrahlung transport spectrum for the each individual mono-energetic beam, one can deduce the information of the RE energy from the HXR spectrum [10].

This work was supported in part by a Grant-in-Aid for Scientific Research 19H01874, and Fund for the Promotion of Joint International Research 17KK0132 from the Japan Society for the Promotion of Science (JSPS).

The views and opinions expressed herein do not necessarily reflect those of the ITER Organization. ITER is a Nuclear Facility INB-174.

- [1] A. Shevelev, V. Kiptily, I. Chugunov, E. Khilkevitch, D. Gin, D. Donikov, V. Naidenov, V. Plyusnin and E.-J. contributors, AIP Conf. Proc. **1612**, 125 (2014).
- [2] A.M. Fernandes *et al.*, IEEE Trans. Nucl. Sci. **61**, 1209 (2014).
- [3] S.P. Pandya, L. Core, R. Barnsley, J. Rosato, R. Reichle, M. Lehnen, L. Bertalot and M. Walsh, Physica Scripta **93**, 115601 (2018).
- [4] J. Sinha, P.C. de Vries, L. Zabeo, E. Veshchev, S.P. Pandya, A. Sirinelli, A. Pironti, G. Vayakis, R.A. Pitts, S.D. Pinches, Y. Gribov and X. Bonnin, Plasma Phys. Control. Fusion **63**, 084002 (2021).
- [5] S.P. Pandya, Ph.D. thesis "Development and performance assessment of ITER Diagnostics for Runaway Electrons based on predictive modelling" (Aix-Marseille Univ., 2019) 2019AIXM0036.
- [6] S. Kajita, E. Veshchev, S. Lisgo, R. Reichle, R. Barnsley,

- M. Walsh, A. Alekseev, A. Gorshkov, D. Vukolov, J. Stuber and S. Woodruff, *Plasma Phys. Control. Fusion* **55**, 085020 (2013).
- [7] S. Kajita, G. Passedat and R. Reichle, *Fusion Eng. Des.* **160**, 111787 (2020).
- [8] N. Yawai, K. Wantong, W. Chewpraditkul, R. Murakami, T. Horiai, S. Kurosawa, A. Yoshikawa and M. Nikl, *Nucl. Instrum. Methods in Phys. Res. Sec. A: Accelerators, Spectrometers, Detectors and Associated Equipment* **844**, 129 (2017).
- [9] E. Hecht, *Optics, 4th edition* (Addison-Wesley, Reading, Mass, 2002).
- [10] A. Patel, S.P. Pandya, A.E. Shevelev, E.M. Khilkevitch and M. Iliasova, "Reconstruction of runaway electron energy distribution function in tokamak discharges using Hard X-ray spectrometry", Research Report (RR)-1314, Library Institute for Plasma Research, Gandhinagar, India, November-2021.